Acta Biomaterialia 35 (2016) 305–317

Contents lists available at ScienceDirect

Acta Biomaterialia

journal homepage: www.elsevier.com/locate/actabiomat

Full length article

Bioactivity of sol–gel-derived TiO_2 coating on polyetheretherketone: In vitro and in vivo studies

Takayoshi Shimizu [a,*], Shunsuke Fujibayashi [a], Seiji Yamaguchi [b], Koji Yamamoto [c], Bungo Otsuki [a], Mitsuru Takemoto [a], Masako Tsukanaka [a], Takashi Kizuki [b], Tomiharu Matsushita [b], Tadashi Kokubo [b], Shuichi Matsuda [a]

[a] Department of Orthopedic Surgery, Kyoto University Graduate School of Medicine, Kyoto, Japan
[b] Department of Biomedical Sciences, College of Life and Health Sciences, Chubu University, 1200 Matsumoto, Kasugai, Aichi 487-8501, Japan
[c] Research and Education Unit of Leaders for Integrated Medical System, Center for the Promotion of Interdisciplinary Education and Research, Kyoto University, Kyoto, Japan

ARTICLE INFO

Article history:
Received 22 September 2015
Received in revised form 28 January 2016
Accepted 5 February 2016
Available online 6 February 2016

Keywords:
PEEK
Bioactivity
TiO_2
Sol–gel
Sandblast
O_2 plasma

ABSTRACT

A polyetheretherketone (PEEK) surface was modified using a sol–gel-derived TiO_2 coating in order to confer bone-bonding ability. To enhance the bonding strength of the coating layer, pretreatment with either O_2 plasma or sandblasting was performed prior to sol–gel coating. Additionally, post-treatment with acid was carried out to confer apatite (calcium phosphate)-forming ability to the surface. Biomechanical and histological analyses performed using an in vivo rabbit tibia model showed that PEEK surfaces modified with sol–gel-derived TiO_2 and acid post-treatment had better bone-bonding properties than uncoated PEEK surfaces. These modified surfaces also performed well in terms of their in vitro cell responses due to their modified surface chemistries and topographies. Although O_2 plasma or sandblasting treatment were, for the most part, equivocal in terms of performance, we conclude that sol–gel-derived TiO_2 coating followed by acid post-treatment significantly improves the bone bonding ability of PEEK surfaces, thus rendering them optimal for their use in surgical implants.

Statement of Significance

The role of polyetheretherketone (PEEK) as an alternative biomaterial to conventional metallic implant materials has become increasingly important. However, its low bone bonding ability is yet to be resolved. This in vivo and in vitro investigation on the functionalization of PEEK surfaces highlights the utility of this material in clinical interventions that require implants, and may extend range of applications of PEEK.

1. Introduction

Two decades have passed since polyether-ether-ketone (PEEK) emerged as a leading high-performance thermoplastic material that could be used instead of metal implants, particularly with regard to replacements in spine surgery. While PEEK has some clear advantages, such as radiolucency and low elastic modulus that is close to the corresponding value for human bone, concerns have been raised about its low bioactivity due to its chemical inertness [1]. In fact, some clinical reports indicate that PEEK is inferior to titanium over long-term usage [2,3]. Thus, further improvements to the bioactivity associated with PEEK surfaces are required if the clinical potential of this material is to be fully realized.

Several studies have described surface coating approaches aimed at increasing the bioactivity of PEEK surfaces; these include plasma-sprayed hydroxyapatite (HA) and titanium coating [4–7]. However, HA coatings are susceptible to degradation over long time periods [8] and there are enduring concerns regarding titanium and its low bonding strength; this is since titanium requires a thick coating layer [6]. In contrast, the sol–gel method provides extremely thin uniform oxide layers that are deposited on the material surface and never degrade [9]. Furthermore, the temperature used in the process of sol–gel coating is significantly lower than the above-mentioned coating technique and, therefore, does not exceed the glass transition temperature of PEEK (about

* Corresponding author at: Department of Orthopedic Surgery, Kyoto University Graduate School of Medicine, 54 Kawahara-cho, Shogoin, Sakyo, Kyoto 606-8507, Japan.
E-mail address: takayosh@kuhp.kyoto-u.ac.jp (T. Shimizu).

http://dx.doi.org/10.1016/j.actbio.2016.02.007
1742-7061/

143 °C). We have previously reported the bioactivity of the sol–gel derived TiO_2 layer on polyethylene terephthalate (PET) in vivo [10]. To our knowledge, however, there have been no publications investigating the effect of sol–gel-derived TiO_2 layers on PEEK surfaces.

Material bioactivity (which hereafter is used to describe its bone-bonding ability in vivo), is often evaluated using the response of osteoblasts or mesenchymal stem cells (MSC) in surrogate in vitro assays. These cellular responses reflect the surface characteristics of materials including both surface chemistry and topography [11–13] and are, therefore, useful for the preliminary evaluation of the surface characteristics. However, prediction of clinical in vivo bone bonding ability is most robustly estimated using animal models. Since the first development of bioactive glass ceramic material in 1991 [14], however, we have presented the theory that the most effective in vitro predictor of in vivo bone bonding ability is the apatite (calcium phosphate)-forming ability of material surfaces in simulated body fluid (SBF) [15]. Recently, we found that adding a sol–gel-derived TiO_2 layer to PEEK confers apatite forming ability in SBF if an acid post-treatment step is performed [16]. In the report, O_2 plasma pretreatment was applied before the sol–gel coating to ensure that the sol–gel layer adhered strongly to the PEEK surface. In the current study, we also evaluated whether sandblasting of TiO_2 particles onto PEEK could be an alternative pretreatment option that could facilitate the adhesion of sol–gel layers.

The aims of this study were (1) to evaluate the in vivo bone bonding ability of a sol–gel derived TiO_2 layer that was pretreated with either O_2 plasma or sandblasting and post-treated with acid, and (2) to determine the surface characteristics of TiO_2 layers and the cellular responses elicited by these surfaces; particular attention was focused on evaluating the apatite-forming ability of the surfaces.

2. Materials and methods

2.1. TiO_2 layer coating

Two types of form, a disc-shaped type measuring 18 mm × 2 mm or a plate-shaped type with 15 mm × 10 mm × 2 mm were cut from the PEEK substrate (TECAPEEK natural, Ensinger Gmbh, Germany: Poisson's ratio 0.4, specific gravity 1.3, flexural modulus 4.2 GPa, tensile strength 97 MPa) and used for in vitro and in vivo studies, respectively. These PEEK materials were coated with TiO_2 using one of 5 distinct processes, as described in Table 1 (Fig. 1A). The BH group, which was not coated with sol–gel, was included in this study because the sandblasted TiO_2 layer alone might have bioactivity following acid post-treatment.

2.1.1. Pretreatment before sol–gel TiO_2 coating (O_2 plasma or sandblast treatment)

PEEK materials were polished with 800 grit Sic paper and then washed sequentially with 2-propanol and ultrapure water in an ultrasonic cleaner for 30 min. After polishing, substrates were subjected to O_2 plasma treatment or sandblast treatment before coating via the sol–gel method. In the O_2 plasma treatment, substrates were placed in the chamber of a polymerization system (PD-10S, SAMCO Inc., Japan). Microwave plasma at 100 watts was applied in an O_2 atmosphere with 50 Pa pressure for 5 min. In the sandblast treatment, TiO_2 particles with a median diameter of 7.62 μm (TOHO Titanium, Kanagawa, Japan) were blasted using a blast-gun with a pressure of 0.5 MPa for 30 s.

Table 1
PEEK implants and associated TiO_2 coating methods.

PEEK implants	Pretreatment	Sol–gel TiO_2 coating	Acid (HCl) post-treatment
Uncoated	–	–	–
OS	O_2 plasma	+	–
OSH	O_2 plasma	+	+
BH	Sandblast	–	+
BSH	Sandblast	+	+

2.1.2. Sol–gel TiO_2 coating and post-treatment with acid (HCl)

After either pretreatment, PEEK materials were dipped into the TiO_2 sol solution consisting of titanium tetraisopropoxide (TTIP), H_2O, ethanol (EtOH), and nitric acid (HNO_3) with a TTIP:H_2O:EtOH:HNO_3 molar ratio of 1:1:37:0.1. The substrates were removed from the solution after 1 min at a rate of 1 cm/min and then air-dried at 80 °C for 24 h. After drying, materials were soaked in 0.1 M HCl solution at 80 °C for 24 h and then gently washed with ultrapure water.

2.2. Surface characterization

2.2.1. Scanning electron microscopy (SEM)

Surface morphology and titanium distribution of coated and uncoated PEEK samples were examined by SEM with Energy Dispersive X-ray Spectroscopy (EDX) (S-4700; Hitachi Ltd, Tokyo, Japan) after coating with Pt/Pd.

2.2.2. Water contact angle

The hydrophobic characteristics of PEEK samples were determined by measuring the water contact angle. A 4-μL droplet of ultrapure water was dropped onto the surface using a microsyringe. The shape of the droplet was observed and the contact angle was measured from a photographic image.

2.2.3. Zeta potential measurements

The zeta potential of the PEEK materials was measured using a zeta potential analyzer (ELS-Z1, Otsuka Electronics Co., Japan). A rectangular PEEK specimen 33 × 15 mm^2 in size and 1 mm in thickness, which was coated with the TiO_2 gel layer, was used for the zeta potential measurement. Dispersant monitoring particles of polystyrene latex (size = 500 nm) coated with hydroxyl propyl cellulose were used. The zeta potential was measured with an applied voltage of 60 V in 10 mM NaCl solution.

2.2.4. Surface roughness (micrometer scale)

A contact probe profilometer (Mitutoyo Surftest SV-2000) was used to measure the topography of the surface coatings of the micrometer scale. We note that this profilometer does not give the submicron-scale roughness measurements that were observed in SEM images because the probe has a 2-μm edge width, which lowers the resolution. The average surface roughness (Ra) of implants coated with each method was measured. Ra in the direction perpendicular to the polished direction was measured at five areas of each implant. The average Ra was calculated from these five areas, and is represented as the sample mean ± standard deviation.

2.2.5. Apatite-forming ability of surfaces

The apatite-forming ability of the samples was examined by soaking them in SBF [15,16] at pH 7.40 for 3 d at 36.5 °C. Soaking at 36.5 ± 0.5 °C is recommended by ISO 23317, and SBF has been shown to generate reproducible results [17]. The ion concentrations (all in mM) were as follows: Na^+, 142.0; K^+, 5.0; Ca^{2+}, 2.5; Mg^{2+}, 1.5; Cl^-, 147.8; HCO^{3-}, 4.2; HPO_4^{2-}, 1.0; SO_4^{2-}, 0.5. The samples were removed from the SBF, washed with distilled water, and dried on a clean bench. Their surfaces were examined with SEM and SEM–EDX, and apatite formation was determined by

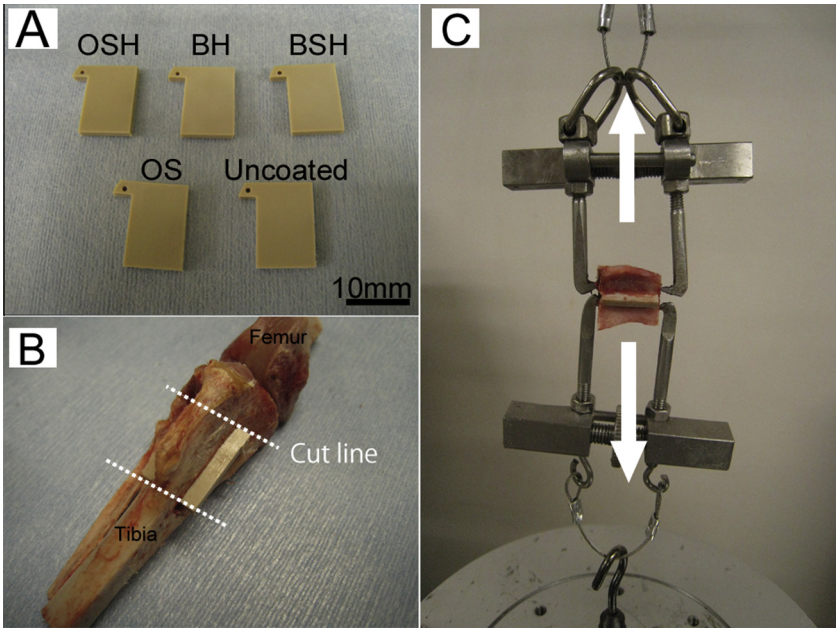

Fig. 1. PEEK sample and mechanical tests used in the in vivo studies. (A): PEEK plates used in vivo. Sandblast-pretreated surfaces (BH and BSH) were slightly white tinged. (B): PEEK plate inserted in the proximal tibia. (C): Detaching test to measure the bonding strength. (Tensile force was applied in the direction as shown by the white arrows).

the presence of spherulites consisting of tiny flake-like crystals, which are the characteristic morphologies of apatite deposited from SBF.

2.3. In vitro study

2.3.1. Isolation, expansion and characterization of bMSCs

Bone mesenchymal stem cells (bMSCs) were isolated from the bone marrow of the femur of four-week-old Japanese white rabbits. The femurs were first separated from the hind legs, followed by removal of the epiphyseal heads and subsequent flushing of the bone marrow plug using α minimum essential medium (α-MEM, Gibco, USA) with 10% fetal bovine serum, 1% penicillin/streptomycin, and 1% heparin. The isolated RBMSCs were cultured in cell culture flasks at 37 °C in a humidified atmosphere of 5% CO_2. The medium was changed four days after seeding, and then changed every two or three days until the cells reached 80% confluence. The experiments with bMSCs were carried out within five passages. For the in vitro cell tests, disk-shaped PEEK substrates were sterilized with ethylene oxide gas. It was previously demonstrated that ethylene oxide sterilization had no adverse effects on the surface coating [10].

At the third passage level, bMSC surface marker expression profiles were characterized using flow cytometry (BD FACS Canto II; Becton Dickinson San Jose, CA) with the following mouse or anti-human antibodies: anti-CD45-FITC (Tonbo Bioscience, San Diego, CA, USA), anti-CD34-FITC (Bioss Inc, MA, USA), anti-CD90-PE (AbD Serotec, USA), anti-CD73-PE (BD Pharmingen, San Diego, CA, USA), and anti-CD105-APC (Miltenyi Biotec, Bergisch-Gladbach, Germany). Additionally, the proliferative and replicative potential of the bMSCs was determined by the colony-forming unit fibroblast (CFU-f) assay. Different numbers of MSCs (10^3, 10^4, 10^5, and 10^6 cells) were incubated on a 6-well plate for 14 d and colony formation was assessed after crystal violet staining. To evaluate the proliferative potential, cell numbers after incubation for 2, 4, and 6 d on a 12-well plate were calculated by measuring the absorbance at 590 nm using a microplate-reader (Multiskan JX, Thermo Labsystems, USA) after crystal violet staining.

2.3.2. Cell adhesion

The bMSCs were seeded on the samples at densities of 1×10^5, 1×10^4, and 0.5×10^4 cells/cm^2 for cell attachment, and then the cells were cultured on the PEEK with the same medium. After 3 h of culturing, the cells were fixed with 4% paraformaldehyde in phosphate buffered saline (PBS) for 10 min, washed in PBS, and permeabilized with 0.1% Triton X-100 in PBS for 10 min. Then the cells were rewashed with PBS and stained with phalloidin for 45 min. Cell attachment was observed using confocal laser scanning microscopy (Nikon D-Eclipse C1 confocal microscope; Nikon, Tokyo, Japan).

2.3.3. Cell viability

After culture on PEEK surfaces for 5 d, bMSCs viability was determined using the XTT assay. The assay is based on the cleavage of the yellow tetrazolium salt, XTT, to an orange formazan dye by metabolically active cells. The bMSCs were seeded onto samples on 12-well plates at 1×10^5 cells/cm^2, and then the cells were cultured on PEEK with the same medium. After 5 d, XTT labeling reagent (Roche Applied Science, IN, USA) was added to each well. After incubation for 4 h, 150 μL of the medium was transferred to a 96-well plate for measurement. The amount of formazan product was quantified by measuring absorbance at 450 nm using a microplate reader (Multiskan JX, Thermo Labsystems, USA).

2.3.4. Alkaline phosphatase (ALP) activity

Cellular differentiation was assessed by measuring ALP activity using p-nitrophenyl phosphate (pNPP) (Wako Pure Chemical Industries, Ltd., Osaka, Japan). The bMSCs were seeded onto the samples in 12-well plates at 1×10^4 (7 d culture) or 0.5×10^4 -cells/cm^2 (14 d culture). After incubation with pNPP at 37 °C for 30 min, the optical density at 405 nm for each sample was measured, and ALP activities were calculated by extrapolation from a standard curve. The ALP levels were normalized to the total protein content and described as μM/mg protein.

2.3.5. Real-time quantitative PCR (RT-qPCR) analysis

The osteogenic differentiation-related genes (ALP, BMP-2, COL1A1, and COL2A1) were analyzed by RT-qPCR. The bMSCs were

Table 2
Primer pairs used in RT-qPCR analysis.

Gene	Forward primer	Reverse primer
GAPDH	GGAATCCACTGGCGTCTTCA	GGTTCACGCCCATCACAAAC
ALP	CATCTCCCCTCTGGAACTCA	CCAAACAGGAGAGTCGCTTC
BMP-2	CGTGAGGATTAGCAGGTCTTTG	CGCTTGACGCTTTTCTCTTCTG
Col1	GGAAACGATGGTGCTACTGG	CCGACAGCTCCAGGGAAG
Col2	GGATAGACCCCAACCAAGGC	GTAGGTGATGTTCTGGGAGC

seeded at a density of 2×10^4 cells/disc in the above-mentioned normal medium and incubated in a humidified incubator for 14 d. Total RNA was then extracted using the RNeasy Mini Kit (Qiagen, Hilden, Germany) according to the manufacturer's instructions. From each sample, RNA was reverse-transcribed with ReverTra Ace qPCR RT Master Mix (TOYOBO, Japan). RT-qPCR was performed using the carousel-based LightCycler system (Roche) with THUNDERBIRD SYBR qPCR Mix (TOYOBO, Japan). The primer sequences used are listed in Table 2. The expression levels of osteogenic differentiation related genes were evaluated and normalized to the internal standard gene (GAPDH).

2.4. In vivo study

2.4.1. Animals

Seventy-five mature male Japanese white rabbits (weight: 2.8–3.5 kg) were used in this study with ethical consent from the Animal Research Committee, Graduate Scholl of Medicine, Kyoto University, Japan. Forty-five of 75 rabbits were used for biomechanical testing, and the remaining 30 were used for histological and radiological analysis. Animals were based on three experimental time-points (4-, 8-, and 16-week groups) with 15 animals (30 legs) in each group for biomechanical testing of 5 implants ($n = 6$), and 10 animals (20 legs) in each group for histological and radiological analyses of 5 implants ($n = 4$).

2.4.2. Surgical procedure, necropsy, and explantation

The PEEK implants were sterilized with ethylene oxide gas. The surgical methods used have been described previously [18]. In brief, the rabbits were anesthetized with an intravenous injection of pentobarbital sodium (40 mg/kg), an inhalation of isoflurane, and local administration of 1% lidocaine solution. A 3-cm longitudinal skin incision was made on the medial side of the knee, and the fascia and the periosteum were incised and retracted to expose the tibial cortex. A 16 mm × 2 mm slit-like perforation was cut using a dental bur from the medial to the lateral cortex within the proximal metaphysis of the tibiae, parallel to the longitudinal axis of the tibiae. After the hole was irrigated with saline, each coated PEEK plate was implanted (Fig. 1B). After irrigation, the fascia and the skin were sutured layer by layer. Animals were housed individually in standard rabbit cages and fed standard rabbit food and water.

At 4, 8, and 16 weeks post-operation, 15 rabbits were sacrificed with an overdose of intravenous pentobarbital sodium in order to examine the biomechanical effects of the implants. Following euthanasia, segments of the proximal tibial metaphyses containing the implanted plates were cut and prepared for biomechanical testing. All the specimens were kept moist after harvesting. To remove periosteal bone growth, the bone tissue surrounding the plates was carefully removed from both sides and the ends using a dental bur.

For histological and radiological analysis, an additional 10 rabbits were sacrificed at 4, 8, and 16 weeks postoperatively.

2.4.3. Biomechanical testing

The detaching test was performed within 24 h of explantation. The detaching test protocol was based on the procedures developed by Nakamura et al. [18]. Traction was applied vertically to the implant surface at a cross-head speed of 35 mm/min using an Instron-type autograph (Model 1011; Aikoh Engineering Co. Ltd., Nagoya, Japan) with specially designed hooks to hold the bone-plate-bone construct (Fig. 1C). The detaching failure load was measured when the plate detached from the bone. If the plate detached before the test, the failure load was defined as 0 N.

After the detaching test, in order to observe onto which side (plate or tibia) the newly formed bone attached, specimens were prepared for surface analysis by SEM (S-4700; Hitachi Ltd, Tokyo, Japan) and EDX. The specimens were washed in sodium hypochlorite solution to remove soft tissue, fixed in 10% phosphate-buffered formalin (pH 7.25) for 3 d, and dehydrated in serial concentrations of ethanol (70%, 80%, 90%, 99%, 100%, and 100% [v/v]) for 1-d each. They were then soaked in isopentyl acetate solution for 1 d, dried in a critical-point drying apparatus (Hcp-2; Hitachi Ltd., Tokyo, Japan), and coated with carbon. All surfaces of the plate and tibia were then examined by SEM with Energy Dispersive X-ray Spectroscope (EDX).

2.4.4. Radiological analysis

After harvesting the tibia of 10 rabbits, a μ-CT scan (SMX-100CT-SV-3; Shimadzu Corp., Kyoto, Japan) with a slice thickness of 0.04 mm was taken. Three-dimensional images of harvested bone including PEEK implants were reconstructed using a software package provided by the manufacturer (VG studio MAX 2.2, Volume Graphics GmbH, Heidelberg, Germany). To measure the new bone volume (NBV) formed surrounding the implants, the region of interest was determined as a sphere of radius 2.5 mm within cancellous bone of the same tolerance and condition. The NBV was defined as the region with the same density as the cortical bone within the sphere.

2.4.5. Histology

After the μ-CT scan, the specimens were fixed in 10% phosphate-buffered formalin (pH 7.25) for 10 d, dehydrated in serial concentrations of ethanol (70%, 80%, 90%, 99%, 100%, and 100% [v/v]) for 3 d at each concentration, and embedded in polyester resin. Thick sections (500 μm) were cut with a band saw (BS-3000CP, EXACT cutting system; Exakt Apparatebau GmbH, Norderstedt, Germany) perpendicular to the tibial axis and then ground to a thickness of 80 μm by using a grinding–sliding machine (Micro-grinding MG-4000; Exakt Apparatebau GmbH). Each section was then stained with Stevenel's blue and van Gieson's picrofuchsin, which differentially stain calcified bone bright red (with the intensity depending on the maturity of the bone), non-calcified bone and osteoid green, and soft tissue blue [19,20]. Thorough microscopic analysis was performed on the histological slides using a transmitted light microscope (Eclipse 80i; Nikon, Tokyo, Japan) with a digital camera (DS-55M-L1; Nikon, Tokyo, Japan). The stained sections were evaluated by quantitative histomorphometry for the amount of direct bone contact to the PEEK implant surface; bone implant contact (BIC),using the 2-dimensional (2-D) image processing software (Image J; National Institutes of Health, Bethesda, MA, USA). The BIC was calculated after the tissue-implant contact area had been manually defined.

2.5. Statistical analysis

Four samples of each of the five implant groups were used for each experiment ($n = 4$), except for biomechanical testing, where six of each of the five implant types were tested ($n = 6$). Statistically significant differences between the 5 groups were measured using one-way analysis of variance (ANOVA) and Tukey's multiple comparison tests. $p < 0.05$ was considered significant. All the statistical analysis was performed using JMP software (version 8.02, SAS Institute, Cary, NC, USA).

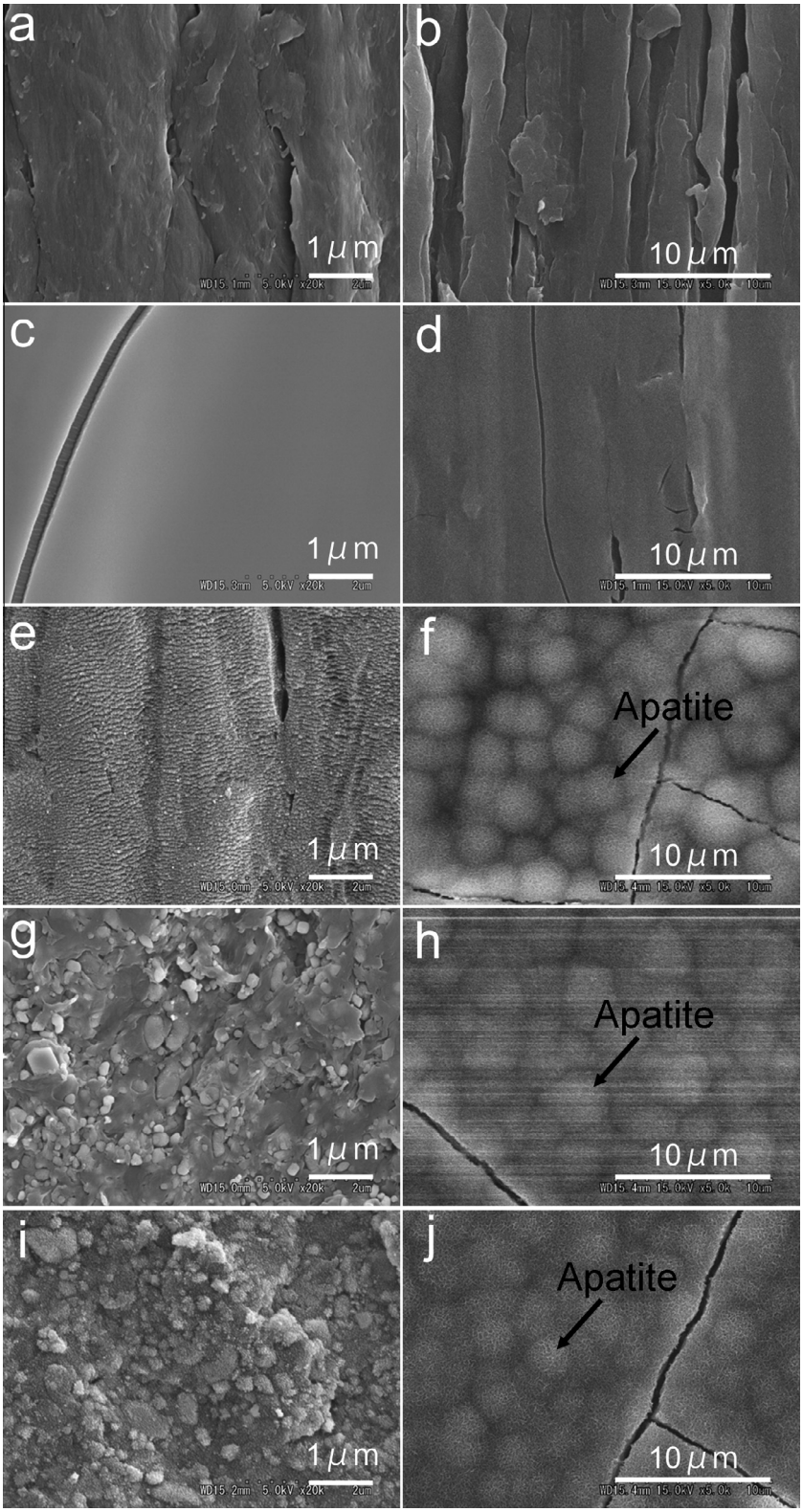

Fig. 2. SEM images of surface-coated PEEK samples. (a) Uncoated PEEK, showing polishing traces on the surface, (b) uncoated PEEK, after soaking in SBF. (c) OS, showing the smooth sol–gel coating layer (d) OS, after soaking in SBF. (e) OSH, showing fine precipitation on the surface, (f) OSH, after soaking in SBF (g) BH, showing a nano-scale rough surface, (h) BH, after soaking in SBF. (i) BSH, showing fine precipitation on a nano-scale rough surface (j) BSH after soaking in SBF. Dome-shaped apatite formation was observed in the OSH, BH, and BSH groups (f, h, j).

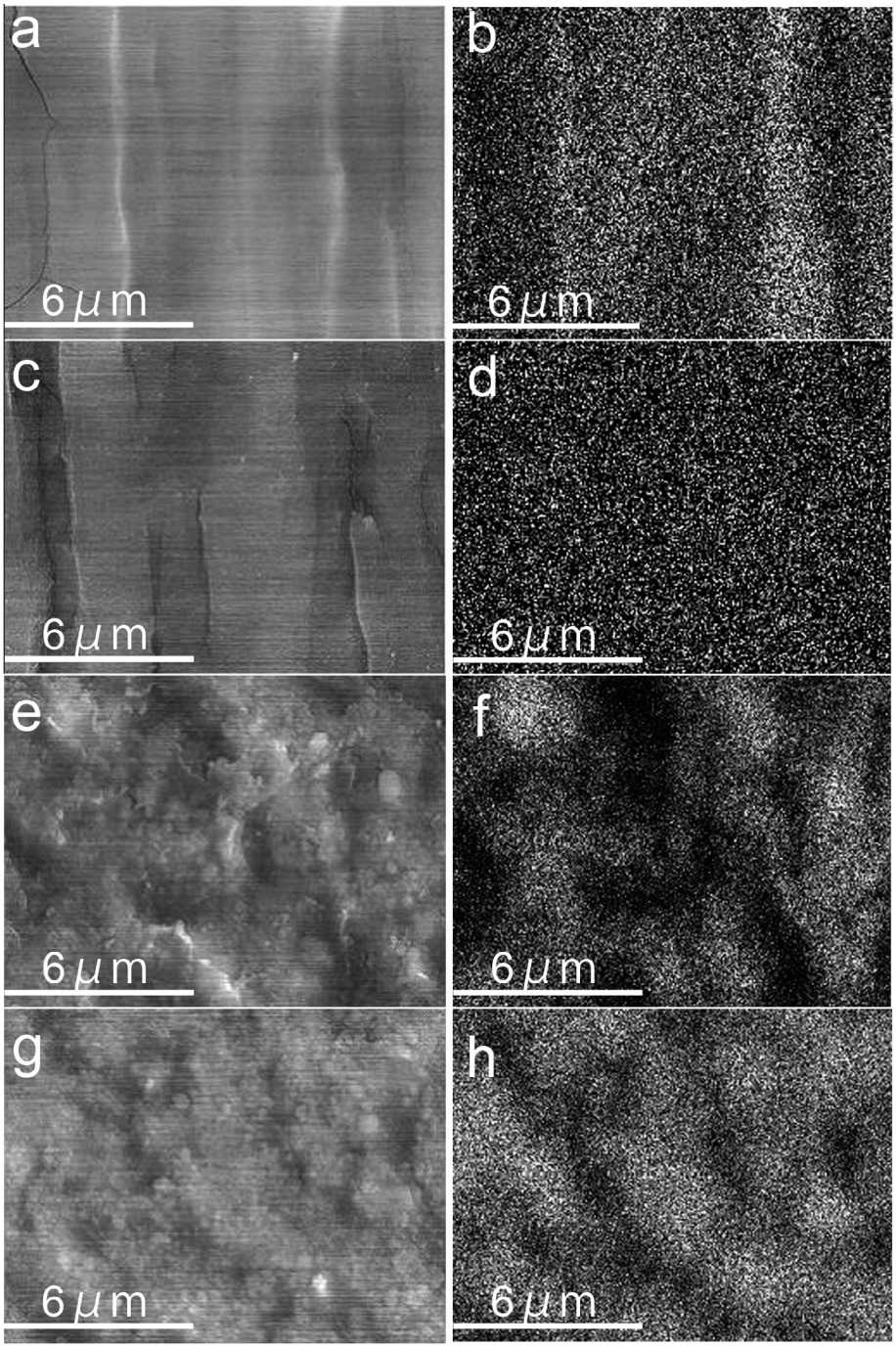

Fig. 3. The titanium distributions of coated surfaces. (a, c, e, g) SEM images of OS, OSH, BH, BSH, respectively. (b, d, f, h) Titanium distribution by EDX for (a, c, e, g), respectively. A non-uniform titanium distribution exists in OS and BH group (b, f). The non-uniformity was improved by acid post-treatment (d) and a sol–gel coating with acid post-treatment (h).

3. Results

3.1. Surface characterization

SEM images of the surfaces of 5 implants are shown in Fig. 2. Uncoated PEEK showed polishing traces on its surface (Fig. 2a). These polishing traces were smoothly coated following a sol–gel coating with O_2 plasma pretreatment (Fig. 2c). Subsequently, nanometer fine particles precipitated following acid post-treatment (Fig. 2e). On the other hand, the surface of sandblast-pretreated PEEK apparently had nano-scale roughness that was created by blasted TiO_2 particles (Fig. 2g, i). Dome-shaped apatite formation was observed in acid post-treated groups (OSH, BH, and BSH (Fig. 2f, h, j) after soaking in SBF, but was not observed in uncoated or OS samples (Fig. 2b, d). The TiO_2 distributions of coated surfaces are shown in Fig. 3. In the OS group, the grooves on the surface derived from polishing were more likely to be covered by TiO_2 than the other areas (Fig. 3b). This non-uniformity was improved in the OSH group due to the acid post-treatment (Fig. 3d). The non-uniformity of TiO_2 distribution was also observed in the BH group (Fig. 3f), and was also improved by sol–gel coating with acid post-treatment (Fig. 3h).

Table 3 shows the surface roughness, wettability, and zeta potential of each implant. At the micrometer scale, surface

Table 3
Surface characteristics of PEEK implants.

PEEK implants	Water contact angle (°)	Zeta potential	Roughness (Ra) ± SD	Apatite-forming ability
Uncoated	92.3	Negative	0.20 ± 0.008	–
OS*	86.6	−16 ± 6.3 (negative)	0.11 ± 0.020	–
OSH*	18.3	8 ± 2.7 (positive)	0.14 ± 0.013	+
BH	59.0	Positive	0.13 ± 0.008	+
BSH	41.0	Positive	0.13 ± 0.011	+

* With the exception of Ra, data for OS and OSH treatments are quoted from our previous report [16].

roughness slightly decreased after both sol–gel and sandblast treatment. From this result, we infer that the sol–gel layer was relatively smooth at micro-scale before acid post-treatment, and that sandblast pretreatment scraped the micro-scale rough pattern from the uncoated, polished PEEK surface. We note that the nano-scale roughness observed in SEM images was not detected by the contact probe profilometer used in this study. The water contact angle of the acid post-treated PEEK surface dramatically decreased compared to implants without acid post-treatment (18.3°, 59.0°, and 41.0° versus 86.6° and 92.3°). These data indicate an increased hydrophilicity of the surface. In fact, the zeta potentials of the acid post-treated surfaces were positively charged. We also note that the difference of the water contact angle between OSH and BSH may be due to the partially exposed sandblast surface on BSH.

3.2. Characterization of bMSCs and in vitro cell responses

Colony formation representing the replication potential of bMSCs was confirmed using a CFU-f assay (Fig. 4a, b). In addition, the gradual increase of cell numbers over the incubation period confirmed the proliferation potential of our bMSCs (Fig. 4c). Flow cytometry analysis showed that our MSCs were negative for CD34, 45, 73, and 90, and positive for CD105 (Fig. 4d). CD34 and 45 are specific to hematopoietic cells and are not expressed on MSCs. On the other hand, CD73, 90, and 105 are considered to be positive for human MSCs, however rabbit MSCs express different surface markers from human MSCs and CD73 and 90 negative [19]. On the basis of these findings, our rabbit bMSCs exhibit characteristics consistent with those of mesenchymal stem cells.

Fig. 5 shows the image of the bMSCs cultured on each implant for 3 h. Slight spreading of actin filaments (red) was observed in O_2 plasma-pretreated groups (OS and OSH), while extensive spreading was seen in sandblast-pretreated groups (BH and BSH). On the other hand, we observed very poor adhesion of cells to uncoated PEEK.

We examined cellular health cultured after a 5-d culture period using the XTT assay (Fig. 6a). Cell viability in all the coated groups tended to be higher than that of cells seeded on uncoated PEEK, which means non-cytotoxicity by the modified surfaces. In particular, OSH samples promoted a statistically significant increase in viability compared to uncoated PEEK.

The activity of ALP was proportional to the degree of cell spreading (Fig. 6b). Sandblast-pretreated groups (BH and BSH) had higher ALP expression than that observed in uncoated PEEK samples; this reached statistically significant values at each time point. In contrast, OS- and OSH-treated surfaces were no more effective than uncoated PEEK surfaces. On the other hand, ALP gene expression demonstrated the efficacy of OS and OSH in addition to BSH compared to uncoated PEEK during the 14-d incubation (Fig. 6c).

Sandblast-pretreated groups (BH and BSH) exhibited higher BMP-2 gene expression than uncoated PEEK in the early incubation period (7 d); however, this high expression was not maintained for 14 d (Fig. 6d). There was no significant difference in Col-1 and Col-2 gene expression between coated and uncoated PEEK over the periods studied (Col-2 data not shown).

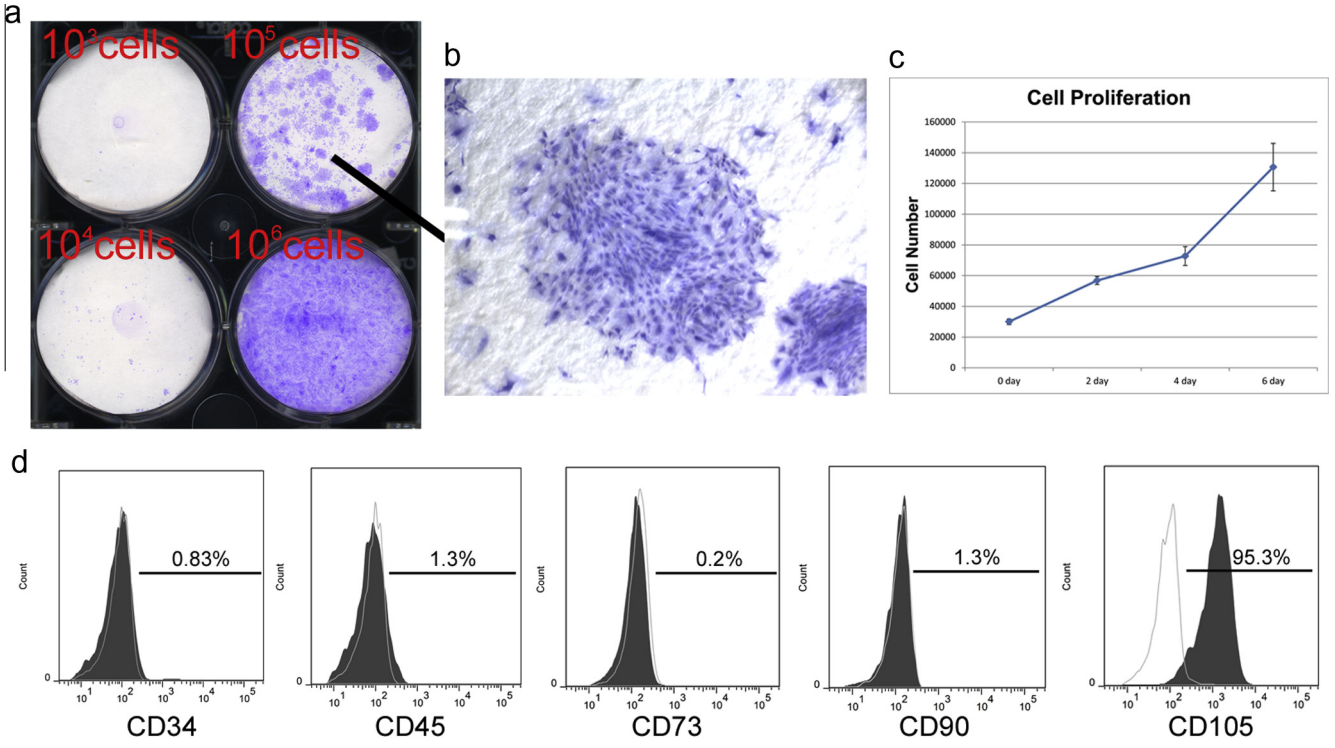

Fig. 4. Confirmation of rabbit bMSC phenotypes. (a, b) CFU-f test showed colony formation consistent with MSC potential. (c) Proliferative potential was confirmed by increase of cell numbers over the incubation period. (d) FACS analysis revealed a CD34$^-$, 45$^-$, 73$^-$, 90$^-$, and 105$^+$ immunophenotype of our rabbit bMSCs (white lines are isotype control).

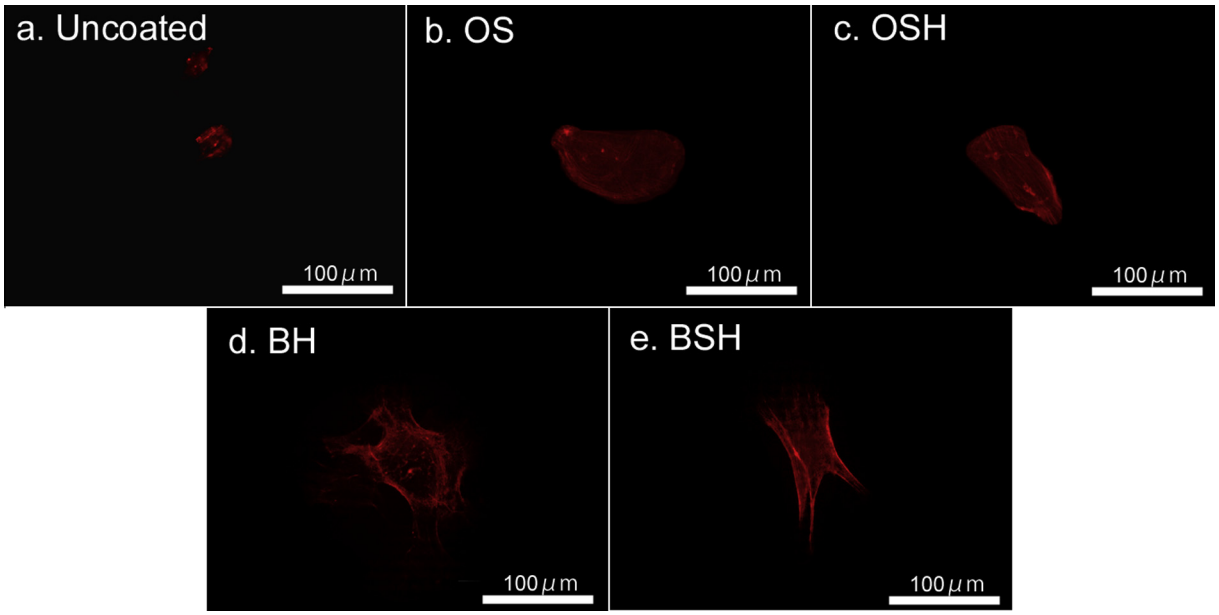

Fig. 5. Cell adhesion (immunostaining of actin filament). (a) Uncoated, small round morphology showing poor adhesion. A moderately stretched cell shape was observed in the OS (b) and OSH (c) groups. Cells were highly stretched, indicative of tight adhesion in the BH (d) and BSH (e) groups.

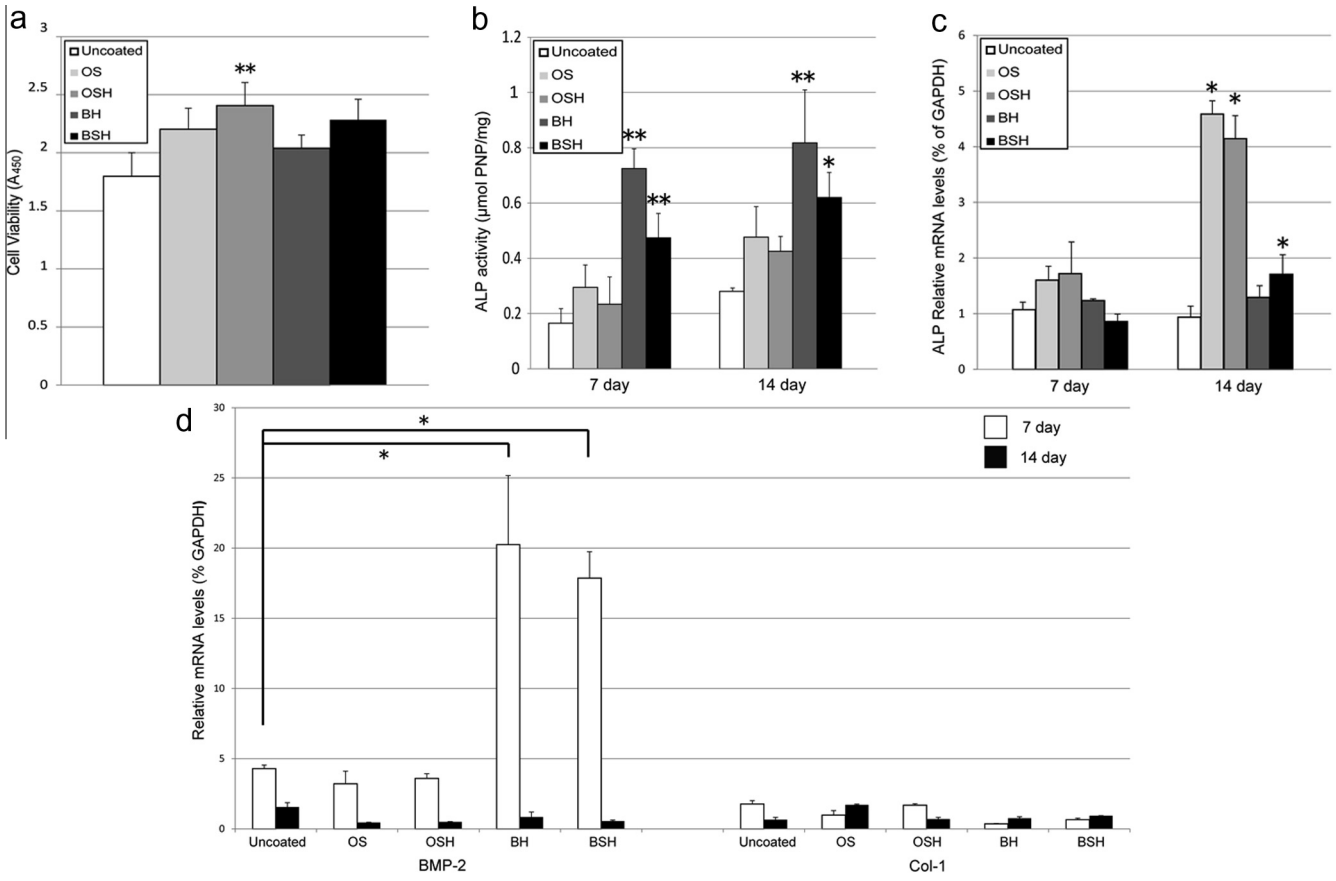

Fig. 6. Viability, ALP activity, and expression of osteogenic genes of MSCs cultured on each sample. (a) OSH-treated surfaces supported a greater cell viability compared to uncoated PEEK surfaces (**: $p < 0.01$). (b) Sandblast pretreatment (BH and BSH) elicited higher ALP activity compared to uncoated PEEK in both time periods (*: $p < 0.05$). (c) OS, OSH, and BSH showed higher ALP expression in 14-d. (d) Sandblast pretreatment (BH and BSH) exhibited higher BMP-2 gene expressions than uncoated PEEK in 7-d incubation, however, these were not maintained for 14-d. There was no significant difference in Col-1 gene expression between the groups.

3.3. In vivo study

The surgical procedures were performed uneventfully in all the animals. No infection of the operated site or implant dislocation was observed during necropsy. No apparent adverse reactions, such as inflammation or foreign body reaction, were found at any of the implanted plates.

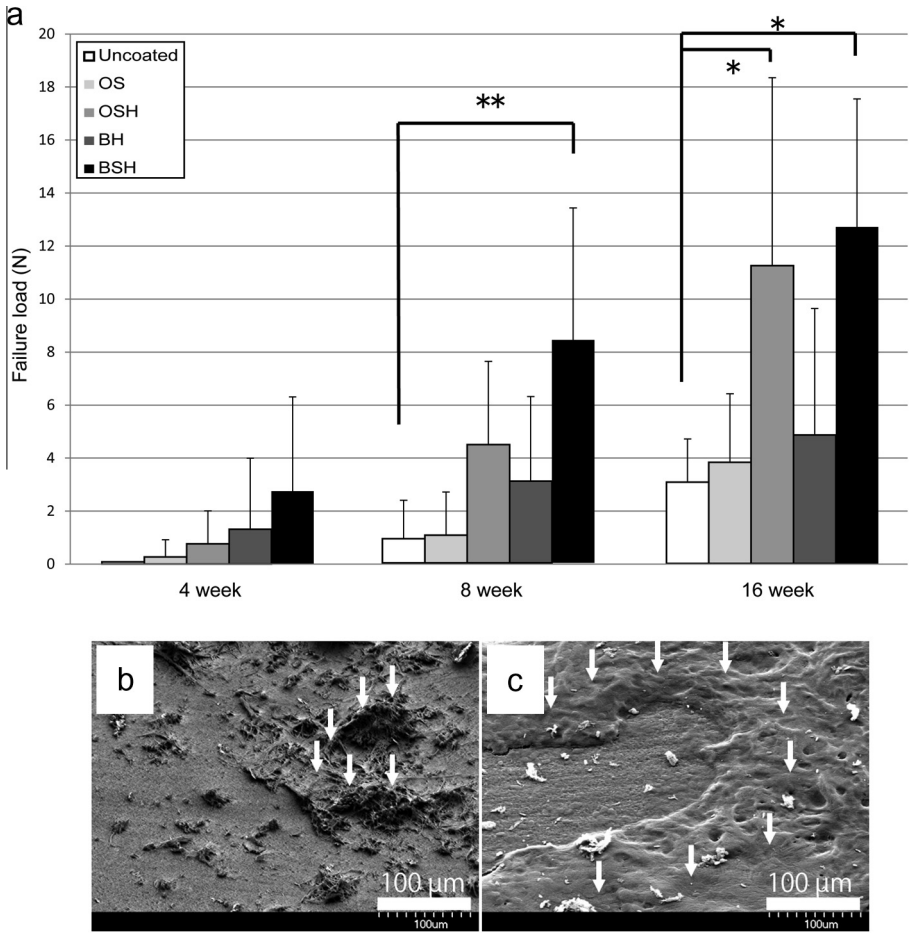

Fig. 7. (a) Detaching test measurement of bonding strength between the PEEK plate and bone measured. BSH showed higher bonding strength compared with uncoated PEEK at 8 weeks. At 16 weeks, BSH and OSH showed higher bonding strengths (*: $p < 0.05$, **: $p < 0.01$). (b, c) Illustrative SEM images after the detaching test. (b) BSH at 4 weeks shows sparse bone residue on the PEEK surface (white arrows). (c) BSH at 16 weeks shows abundant bone residue on the PEEK surface (white arrows).

3.3.1. Biomechanical testing

Fig. 7a shows the findings of the detaching test. There was no statistical difference in failure load between the 5 groups at 4 weeks after implantation. At 8 weeks, the BSH group was associated with a higher bonding strength than uncoated PEEK samples. At 16 weeks, BSH and OSH groups had higher bonding strength than uncoated PEEK samples. OS and BH groups showed no improvement to uncoated PEEK throughout the period studied. Fig. 7b, c shows representative SEM images of the surface of BSH following the detaching test at 4 and 16 weeks. Sparse bone residue was observed on the surface at 4 weeks, which coincided with the low bonding strength reported in the detaching test. In contrast, abundant bone residue remained on the surface at 16 weeks, reflecting the development of high bonding strength. Throughout the time period studied, the surface morphology of PEEK in SEM images was unchanged after the detaching test. This demonstrates that the TiO_2 coating layer remained attached to the PEEK surface.

3.3.2. New bone formation

μ-CT cross-sectional imaging revealed new bone formation surrounding the implants (Fig. 8a). At 8 weeks, thin bone layers were formed around implants within cancellous bone in the OSH and BSH groups; these bone layers grew thicker at 16 weeks. The amount of NBV that formed around PEEK surfaces is shown in Fig. 8b. There was no statistical difference between the 5 implant types at 4 weeks. However, at 8 and 16 weeks, the BSH group was associated with greater NBV than uncoated PEEK surfaces. In addition, there was greater NBV in the OSH group than uncoated PEEK samples at 16 weeks. The OS and BH groups had no greater NBV than uncoated PEEK samples throughout the study. The differences between the groups generally followed a similar trend as those observed in the detaching tests.

3.3.3. Histology and histomorphometry

Fig. 9a shows the results of histological analysis. At 4 weeks, immature bone formation was present around old bone tissue in acid post-treated groups (OSH, BH, and BSH). At 8 weeks, this newly formed bone began to mature in the OSH and BSH groups (but not in the BH group); this coincided with direct contact between new bone and the implant. At 16 weeks, even more mature lamellar bone directly bonded to the PEEK surface in the OSH and BSH groups, while a gap was observed in the BH group. Direct contact was barely observed in the uncoated and OS groups throughout the experiment.

The BIC was calculated as described in the Materials and Methods (Fig. 9b). There was no statistical difference between the 5 groups at 4 weeks. However, at 8 and 16 weeks, the BSH group had greater BIC than animals that received uncoated PEEK implants. The OSH group was associated with greater BIC than the uncoated PEEK group at 16 weeks, while BIC was no different in the OS and BH groups compared to the uncoated PEEK group. Again, this pattern of results was consistent with those regarding detachment and NBV.

4. Discussion

Since its commercial release in 1998, PEEK is now a widely accepted biomaterial, especially in the field of spinal surgery [20]. The continued availability, radiolucency, and biomechanical success of PEEK have ensured its continual clinical usage. The radiolucency of PEEK enables surgeons to easily determine whether postsurgical bony fusion has occurred by the use of a simple radiograph [21]. Additionally, the elastic modulus (flexural modulus 4 GPa in unfilled PEEK) is close to human cortical bone; this likely attenuates the subsidence that is sometimes observed in titanium implants and also encourages bony fusion by generating adequate stress on the grafted bone [22–25]. Despite these advantages, however, the chemical inertness of PEEK reduces the potential for direct bone bonding and forms the connective tissue surrounding the PEEK; this has led to unsatisfactory outcomes in both in vitro and clinical studies [3,26,27]. To overcome this drawback without losing the advantages of PEEK, we applied TiO_2 to the PEEK surface using the sol–gel method in this current study.

Sol–gel derived coating has several advantages compared to other coating methods such as plasma spraying. These include: (1) a simple and cost-effective process, (2) a thinner and uniform coating layer even on substrates with difficult geometries and large surfaces, and (3) the temperature used in sol–gel method is significantly lower (80 °C at maximum in the current study) than those of traditional coating processes [28]. The thickness of the sol–gel TiO_2 layers in cross-sectional surfaces were examined using Field Emission SEM (FE-SEM) equipped with EDX. Although clear images were not obtained, the thickness we estimated from some fragments of broken specimens was approximately 30 nm before acid treatment and 20 nm after acid treatment.

Our coating process is based on the following chemical principles. After O_2 plasma pretreatment, C—O, C=O, and O—C=O groups are formed on the PEEK; these groups have high affinity with the Ti—O group in the TiO_2 gel. In terms of sandblasting pretreatment, TiO_2 particles that physically adhere to the PEEK surface also have high affinity with the Ti—O group in the TiO_2 gel. These chemical bondings render stronger adhesive forces to the sol–gel coating. The bonding strength between a sol–gel derived coating layer and titanium substrates has been proven to be sufficient for their use as implant coating materials (>24 MPa) [29,30]. With regard to the stability of the sol–gel TiO_2 coating layer on PEEK substrates, we evaluated the adhesion of the TiO_2 gel layer to the PEEK substrate with a modified ISO 2409 tape test in a previous study. A sol–gel derived layer adhered to the substrate so firmly that the layer could not be peeled from the substrate by detaching the tape pressed to the surface, due to its dramatically improved hydrophilicity. Prior to the sol–gel coating, the water contact angle of as-polished PEEK surface was 92.3°, however when pretreated with O_2 plasma, the angle was $\leqq 1°$ [16]. Our findings in the current in vivo study showed that the sol–gel derived TiO_2 coating on PEEK substrates remained unchanged after a 16-week period of implantation, demonstrating good bone bonding ability if post-treated with acid, and did not peel off under the conditions of a detaching

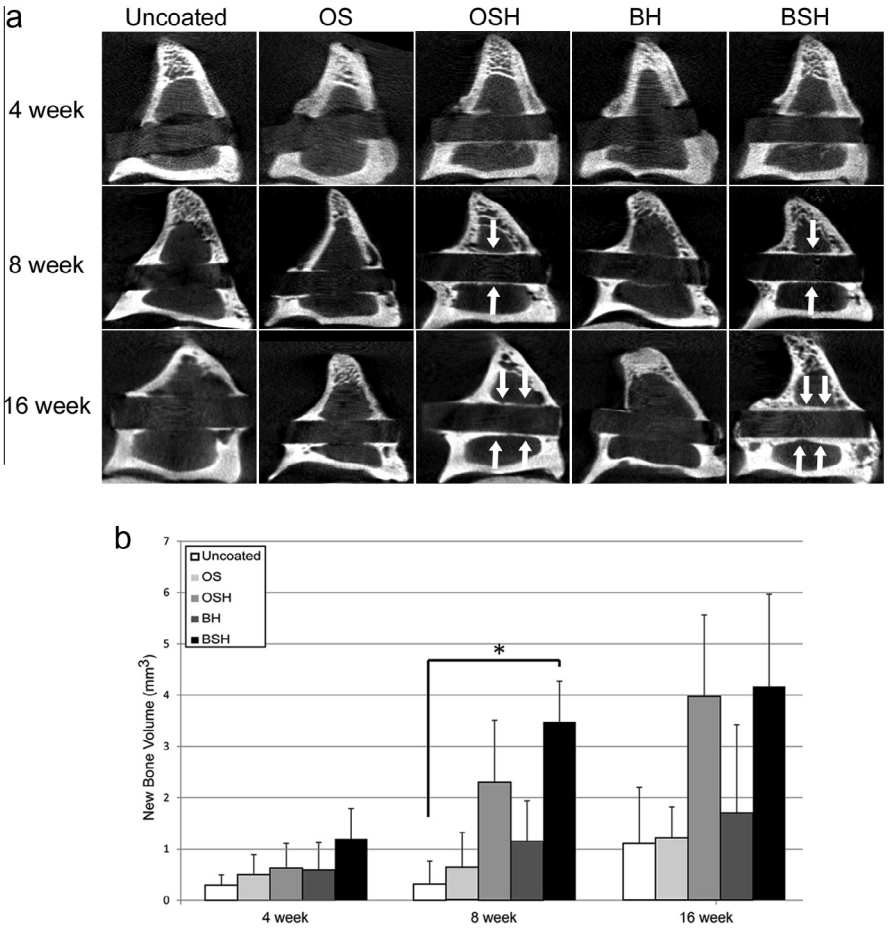

Fig. 8. In vivo μCT imaging. (a) OSH and BSH promoted new bone formation surrounding the PEEK plate at 8 weeks (white arrows). At 16 weeks, the thickness of the new bone deposits increased (white arrows). (b) New bone volume surrounding PEEK plates in vivo. BSH engendered greater new bone formation compared to uncoated PEEK at 8 weeks (*: $p < 0.05$). At 16 weeks, BSH and OSH showed a tendency to increase new bone volume, although this did not reach statistical significance.

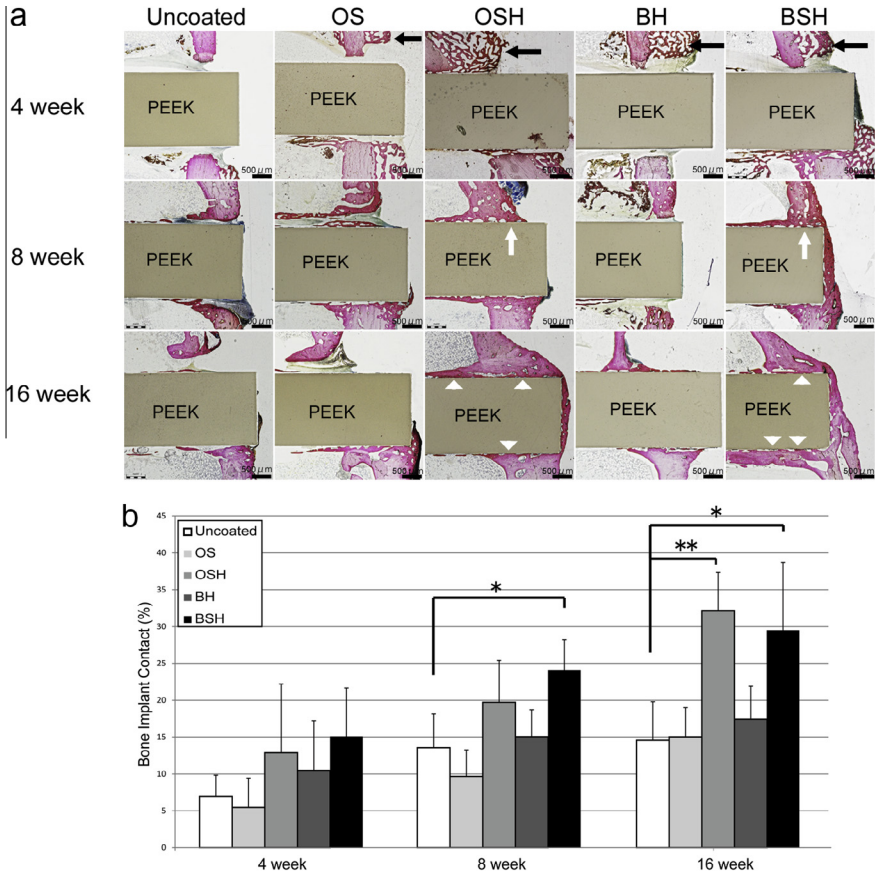

Fig. 9. Histology and histomorphometry. (a) New bone formation was observed at 4 weeks in all groups except for those that received uncoated PEEK (black arrows). At 8 weeks, BSH and OSH showed direct contact between new bone and PEEK (white arrows). At 16 weeks, new bone changed to mature bone and extended contact was observed in the BSH and OSH groups (white arrowheads). (b) Bone implant contact (BIC). BSH treatment elicited greater BIC compared to uncoated PEEK surfaces at 8 weeks. At 16 weeks, BSH and OSH induced higher BIC (*: $p < 0.05$, **: $p < 0.01$).

test. We previously performed similar in vivo biomechanical experiments with titanium. In this situation, we observed failure load of 0–5 N at 4, 8, and 16 weeks after implantation, which was inferior to OSH and BSH PEEK in this study. Nevertheless, a slight concern remains regarding delamination of the layer with O_2 plasma pretreatment in actual surgical situations, such as spine surgery. This is since, in such cases, the PEEK implants are hammered into the interbody space and exposed to extensive friction. Sandblasted TiO_2 particles appeared firmly integrated with the PEEK surface (Fig. 2g, i), and were chemically bonded to the overlying sol–gel-derived TiO_2 layer. In the real surgical situations, sandblast pretreatment may induce better adhesion than O_2 plasma pretreatment. To confirm this hypothesis, further experimental studies that recapitulate the real surgical situation are required.

As a bioactive ceramic, HA is frequently used as a composite or surface coating material to confer bioactivity on PEEK substrates [7,31,32]. Indeed, HA seems promote a high degree of osseointegration as soon as 4 weeks after implantation [5,7]. However, varying levels of HA resorption have been reported in human retrieval studies [33–35]; this is not associated with inorganic oxides, such as TiO_2. Rokkum et al. stated that approximately one-third of the length and thickness of the HA was missing in hip stems, and attributed this to resorption by macrophages and multinucleated giant cells [8]. Indeed, resorption of the coating layer poses one of the greatest threats to the success of clinical interventions that use biomaterial in the orthopedic or spine fields.

Acid post-treatment was used to provide the TiO_2 layer with apatite-forming ability in SBF [36]. We analyzed the structure of the sol–gel derived TiO_2 layer before and after acid treatment on a thicker layer coated on polyethylene terephthalate (PET) by X-ray diffraction, as described in a previous study [37]. According to this report, the sol–gel derived TiO_2 layer had an amorphous structure before acid treatment, and transformed into positively-charged crystalline brookite (10–100 nm in size) accompanied with a small amount of anatase and rutile following acid treatment. The apatite formation of the TiO_2 layer in SBF was attributed to the positive charge of the surface induced by the acid treatment [16]. The positively charged surface absorbs the negatively charged phosphate ions in SBF; this in turn leads to the absorption of positively charged calcium ions and apatite formation. We have advocated that such apatite-forming ability is the most crucial predictor of in vivo bone bonding ability [14,15]. When the apatite layer forms on substrate surfaces in a physiological environment, it more closely resembles bone mineral in composition and structure than does ready-made sintered HA [38]. This physiologic apatite layer serves as a foundation for direct bone bonding. In fact, the uncoated PEEK and OS groups, which do not exhibit apatite-forming ability, showed poor direct bone bonding in our in vivo study. However, the BH group, which stimulates apatite formation, failed to promote bone bonding. This is probably since sandblasted TiO_2 particles alone were not able to cover the entire surface of PEEK, thereby exposing a considerable amount of uncoated surface. This indicates sandblast pretreatment itself cannot be a coating modality that will confer bioactivity to PEEK surfaces.

Cell responses on the material surface are influenced by the two main factors of surface chemistry and topography [39]. In this study,

we evaluated wettability and zeta-potential as two surface chemistry parameters, and measured surface roughness as a topography index. The sol–gel-derived TiO_2 layer drastically increased the wettability when it was followed by acid post-treatment. In addition, a positive surface charge was induced by acid post-treatment, which is known to be favorable to cell adhesion [13]. This highly increased wettability engendered higher cell viability in the OSH group. In terms of cell differentiation, nano/micro-scale roughness induced by the sandblast pretreatment promoted more robust differentiation of MSCs into osteoblasts. This was confirmed by the higher ALP activity and BMP-2 expression in the BH and BSH groups, although the contact probe profilometer used in this study was not able to detect nanoscale roughness, but nano/micro-scale roughness on sandblasted PEEK surfaces was clearly revealed by SEM imaging. However, BMP-2 gene expression was not maintained for long incubation periods, indicating that the osteogenic differentiation of MSCs cannot be maintained in an in vitro non-osteogenic environment and, specifically, a non-apatite environment. These cellular responses are certainly promising in terms of the development of novel bioactive surface modifications. However, it is still unclear whether these in vitro tests can directly predict in vivo bone bonding ability. In fact, expression of osteogenic differentiation-related genes and proteins in vitro did not demonstrate results proportional to in vivo bone bonding ability in this study. In contrast, apatite layer formation in SBF has been proven to certainly exist between newly formed bone and the surface of modified substrates in vivo [40–42]. These findings underscore our hypothesis that apatite-forming ability in SBF is the most reliable predictor of in vivo bone bonding ability.

In summary, surface modification of PEEK with sol–gel derived TiO_2 coating and acid post-treatment yields a biomaterial with higher mechanical bonding strength in vivo. Furthermore, μCT analysis clearly revealed that surface-modified PEEK had good osteoconductivity. There were no significant differences between O_2 plasma pretreatment and sandblast pretreatment in terms of their bone-bonding ability. However, given that these two pretreatments generate different modalities of adhesion, there may be significant differences in their performances pre-clinical experimental studies or over longer implantation periods.

5. Conclusion

Treatments with sol–gel-derived TiO_2 coatings confer greater bone bonding ability to PEEK surfaces. The choice of pretreatment (O_2 plasma or sandblasting) does not appear to impact on the relatively short-term functionality of these improved PEEK surfaces. Additional pre-clinical research into functionalization of PEEK surfaces will ensure that this material remains a mainstay of clinical interventions that require implants, and may extend the range of applications accessible to PEEK.

Acknowledgements

We greatly appreciate the technical support of Mr. Kohda and Ms. Furuta for the SEM studies and Dr. Takayuki Fujii for FACS.

References

[1] S.M. Kurtz, J.N. Devine, PEEK biomaterials in trauma, orthopedic, and spinal implants, Biomaterials 28 (2007) 4845–4869.
[2] J.J. Schimmel, M.S. Poeschmann, P.P. Horsting, D.H. Schonfeld, J. van Limbeek, P.W. Pavlov, PEEK cages in lumbar fusion: mid-term clinical outcome and radiological fusion, J. Spinal Disorders Tech. (2012).
[3] O. Nemoto, T. Asazuma, Y. Yato, H. Imabayashi, H. Yasuoka, A. Fujikawa, Comparison of fusion rates following transforaminal lumbar interbody fusion using polyetheretherketone cages or titanium cages with transpedicular instrumentation, Eur. Spine J. 23 (2014) 2150–2155.
[4] G.M. Wu, W.D. Hsiao, S.F. Kung, Investigation of hydroxyapatite coated polyether ether ketone composites by gas plasma sprays, Surf. Coat. Technol. 203 (2009) 2755–2758.
[5] P. Johansson, R. Jimbo, P. Kjellin, F. Currie, B.R. Chrcanovic, A. Wennerberg, Biomechanical evaluation and surface characterization of a nano-modified surface on PEEK implants: a study in the rabbit tibia, Int. J. Nanomed. 9 (2014) 3903–3911.
[6] D.M. Devine, J. Hahn, R.G. Richards, H. Gruner, R. Wieling, S.G. Pearce, Coating of carbon fiber-reinforced polyetheretherketone implants with titanium to improve bone apposition, J. Biomed. Mater. Res. B Appl. Biomater. 101 (2013) 591–598.
[7] S. Barkarmo, A. Wennerberg, M. Hoffman, P. Kjellin, K. Breding, P. Handa, et al., Nano-hydroxyapatite-coated PEEK implants: a pilot study in rabbit bone, J. Biomed. Mater. Res. A 101 (2013) 465–471.
[8] M. Rokkum, A. Reigstad, C.B. Johansson, T. Albrektsson, Tissue reactions adjacent to well-fixed hydroxyapatite-coated acetabular cups. Histopathology of ten specimens retrieved at reoperation after 0.3 to 5.8 years, J. Bone Joint Surg. Br. 85 (2003) 440–477.
[9] J. Krzak-Ros, J. Filipiak, C. Pezowicz, A. Baszczuk, M. Miller, M. Kowalski, et al., The effect of substrate roughness on the surface structure of TiO(2), SiO(2), and doped thin films prepared by the sol–gel method, Acta Bioeng. Biomech./Wroclaw Univ. Technol. 11 (2009) 21–29.
[10] T. Saito, M. Takemoto, A. Fukuda, Y. Kuroda, S. Fujibayashi, M. Neo, et al., Effect of titania-based surface modification of polyethylene terephthalate on bone-implant bonding and peri-implant tissue reaction, Acta Biomater. 7 (2011) 1558–1569.
[11] L. Bacakova, E. Filova, F. Rypacek, V. Svorcik, V. Stary, Cell adhesion on artificial materials for tissue engineering, Physiol. Res./Acad. Sci. Bohemoslovaca 53 (Suppl 1) (2004) S35–S45.
[12] A. Ochsenbein, F. Chai, S. Winter, M. Traisnel, J. Breme, H.F. Hildebrand, Osteoblast responses to different oxide coatings produced by the sol–gel process on titanium substrates, Acta Biomater. 4 (2008) 1506–1517.
[13] L. Bacakova, E. Filova, M. Parizek, T. Ruml, V. Svorcik, Modulation of cell adhesion, proliferation and differentiation on materials designed for body implants, Biotechnol. Adv. 29 (2011) 739–767.
[14] T. Kokubo, Bioactive glass ceramics: properties and applications, Biomaterials 12 (1991) 155–163.
[15] T. Kokubo, H. Takadama, How useful is SBF in predicting in vivo bone bioactivity?, Biomaterials 27 (2006) 2907–2915
[16] T. Kizuki, T. Matsushita, T. Kokubo, Apatite-forming PEEK with TiO2 surface layer coating, J. Mater. Sci. – Mater. Med. 26 (2015) 5359.
[17] Implants for surgery – in vitro evaluation for apatite-forming ability of implant materials. ISO 23317:2014, 2014.
[18] T. Nakamura, T. Yamamuro, S. Higashi, T. Kokubo, S. Itoo, A new glass–ceramic for bone replacement: evaluation of its bonding to bone tissue, J. Biomed. Mater. Res. 19 (1985) 685–698.
[19] T.C. Lee, T.H. Lee, Y.H. Huang, N.K. Chang, Y.J. Lin, P.W. Chien, et al., Comparison of surface markers between human and rabbit mesenchymal stem cells, PLoS One 9 (2014) e111390.
[20] Invibio Ltd, Thornton-Cleveleys, United Kingdom, 1998.
[21] J.M. Toth, M. Wang, B.T. Estes, J.L. Scifert, H.B. Seim 3rd., A.S. Turner, Polyetheretherketone as a biomaterial for spinal applications, Biomaterials 27 (2006) 324–334.
[22] D. Lau, J.E. Ziewacz, H. Le, R. Wadhwa, P.V. Mummaneni, A controlled anterior sequential interbody dilation technique for correction of cervical kyphosis, J. Neurosurg. Spine (2015) 1–11.
[23] S. Vadapalli, K. Sairyo, V.K. Goel, M. Robon, A. Biyani, A. Khandha, et al., Biomechanical rationale for using polyetheretherketone (PEEK) spacers for lumbar interbody fusion-A finite element study, Spine 31 (2006) E992–E998.
[24] W.J. Wu, L.S. Jiang, Y. Liang, L.Y. Dai, Cage subsidence does not, but cervical lordosis improvement does affect the long-term results of anterior cervical fusion with stand-alone cage for degenerative cervical disc disease: a retrospective study, Eur. Spine J. 21 (2012) 1374–1382.
[25] D. Lau, Y. Song, Z. Guan, F. La Marca, P. Park, Radiological outcomes of static vs expandable titanium cages after corpectomy: a retrospective cohort analysis of subsidence, Neurosurgery 72 (2013) 529–539. Discussion 8–9.
[26] R. Olivares-Navarrete, R.A. Gittens, J.M. Schneider, S.L. Hyzy, D.A. Haithcock, P. F. Ullrich, et al., Osteoblasts exhibit a more differentiated phenotype and increased bone morphogenetic protein production on titanium alloy substrates than on poly-ether-ether-ketone, Spine J. 12 (2012) 265–272.
[27] R. Olivares-Navarrete, S.L. Hyzy, P.J. Slosar, J.M. Schneider, Z. Schwartz, B.D. Boyan, Implant materials generate different peri-implant inflammatory factors: poly-ether-ether-ketone promotes fibrosis and microtextured titanium promotes osteogenic factors, Spine 40 (2015) 399–404.
[28] S. Areva, H. Paldan, T. Peltola, T. Narhi, M. Jokinen, M. Linden, Use of sol–gel-derived titania coating for direct soft tissue attachment, J. Biomed. Mater. Res. A 70 (2004) 169–178.
[29] M.E. Pätsi, J.A. Hautaniemi, H.M. Rahiala, T.O. Peltola, I.M.O. Kangasniemi, Bonding strengths of titania sol–gel derived coatings on titanium, J. Sol–Gel. Sci. Technol. 11 (1998) 55–66.
[30] Guidance Document for Testing Orthopedic Implants with Modified Metallic Surfaces Apposing Bone or Bone Cement. U.S. Food and Drug Administration, April 28, 1994.
[31] J.H. Lee, H.L. Jang, K.M. Lee, H.R. Baek, K. Jin, K.S. Hong, et al., In vitro and in vivo evaluation of the bioactivity of hydroxyapatite-coated polyetheretherketone biocomposites created by cold spray technology, Acta Biomater. 9 (2013) 6177–6187.

[32] X. Wu, X. Liu, J. Wei, J. Ma, F. Deng, S. Wei, Nano-TiO2/PEEK bioactive composite as a bone substitute material: in vitro and in vivo studies, Int. J. Nanomed. 7 (2012) 1215–1225.
[33] R.J. Furlong, J.F. Osborn, Fixation of hip prostheses by hydroxyapatite ceramic coatings, J. Bone Joint Surg. Br. 73 (1991) 741–745.
[34] M.T. Manley, W.N. Capello, J.A. D'Antonio, A.A. Edidin, R.G. Geesink, Fixation of acetabular cups without cement in total hip arthroplasty. A comparison of three different implant surfaces at a minimum duration of follow-up of five years, J. Bone Joint Surg. Am. 80 (1998) 1175–1185.
[35] P. Buma, J.W. Gardeniers, Tissue reactions around a hydroxyapatite-coated hip prosthesis. Case report of a retrieved specimen, J. Arthroplasty 10 (1995) 389–395.
[36] D.K. Pattanayak, S. Yamaguchi, T. Matsushita, T. Kokubo, Nanostructured positively charged bioactive TiO2 layer formed on Ti metal by NaOH, acid and heat treatments, J. Mater. Sci. – Mater. Med. 22 (2011) 1803–1812.
[37] T. Kokubo, T. Ueda, M. Kawashita, Y. Ikuhara, G.H. Takaoka, T. Nakamura, PET fiber fabrics modified with bioactive titanium oxide for bone substitutes, J. Mater. Sci. – Mater. Med. 19 (2008) 695–702.
[38] T. Kokubo, H.M. Kim, S. Nishiguchi, T. Nakamura, In vivo apatite formation induced on titanium metal and its alloys by chemical treatment, in: Key Engineering Materials, Trans Tech Publ., 2000, pp. 3–6.
[39] F.H. Jones, Teeth and bones: applications of surface science to dental materials and related biomaterials, Surf. Sci. Rep. 42 (2001) 75–205.
[40] H. Kato, T. Nakamura, S. Nishiguchi, Y. Matsusue, M. Kobayashi, T. Miyazaki, et al., Bonding of alkali- and heat-treated tantalum implants to bone, J. Biomed. Mater. Res. 53 (2000) 28–35.
[41] S. Nishiguchi, S. Fujibayashi, H.M. Kim, T. Kokubo, T. Nakamura, Biology of alkali- and heat-treated titanium implants, J. Biomed. Mater. Res. A 67 (2003) 26–35.
[42] M. Neo, S. Kotani, T. Nakamura, T. Yamamuro, C. Ohtsuki, T. Kokubo, et al., A comparative study of ultrastructures of the interfaces between four kinds of surface-active ceramic and bone, J. Biomed. Mater. Res. 26 (1992) 1419–1432.